Lab on a Chip

PAPER

View Article Online
View Journal | View Issue

Cite this: *Lab Chip*, 2014, **14**, 315

Biosensor design based on Marangoni flow in an evaporating drop†

Joshua R. Trantum,[a] Mark L. Baglia,[a] Zachary E. Eagleton,[a] Raymond L. Mernaugh[b] and Frederick R. Haselton*[a]

Received 28th August 2013,
Accepted 7th November 2013

DOI: 10.1039/c3lc50991e

www.rsc.org/loc

Effective point-of-care diagnostics require a biomarker detection strategy that is low-cost and simple-to-use while achieving a clinically relevant limit of detection. Here we report a biosensor that uses secondary flows arising from surface Marangoni stresses in an evaporating drop to concentrate target-mediated particle aggregates in a visually detectable spot. The spot size increases with increasing target concentration within the dynamic range of the assay. The particle deposition patterns are visually detectable and easily measured with simple optical techniques. We use optical coherence tomography to characterize the effect of cross-sectional flow fields on the motion of particles in the presence and absence of target (aggregated and non-aggregated particles, respectively). We show that choice of substrate material and the presence of salts and glycerol in solution promote the Marangoni-induced flows that are necessary to produce signal in the proposed design. These evaporation-driven flows generate signal in the assay on a PDMS substrate but not substrates with greater thermal conductivity like indium tin oxide-coated glass. In this proof-of-concept design we use the M13K07 bacteriophage as a model target and 1 μm-diameter particles surface functionalized with anti-M13 monoclonal antibodies. Using standard microscopy-based techniques to measure the final spot size, the assay has a calculated limit-of-detection of approximately 100 fM. Approximately 80% of the maximum signal is generated within 10 minutes of depositing a 1 μL drop of reacted sample on PDMS enabling a relatively quick time-to-result.

Introduction

The engineering of diagnostic devices suitable for the low resource, point-of-care (POC) setting is challenged by design criteria that include low cost, simplicity of operation, and minimal reliance on external instrumentation.[1,2] The ideal biosensor requires no on-board power source and produces an easily detectable signal in a short period of time. Harnessing the hydrodynamics of an evaporating drop represents one possible means of satisfying these design requirements. Fluid motion inside an evaporating sessile drop occurs spontaneously due to a non-uniform evaporation rate along the surface of the drop, which produces predictable hydrodynamic properties.[3–5] The resulting flow fields include primary radial flow and secondary flows caused by direct and indirect effects of the non-uniform evaporation rate, respectively.[3–8]

The primary radial flow field is the most commonly and easily observed flow pattern in an evaporating drop. It is this flow field which causes a ring to form in an evaporating coffee drop, known as the "coffee ring effect".[5] The non-uniform evaporation rate across the surface of the drop induces a radial current that carries material in solution to the periphery of the drop resulting in a concentrated ring pattern.[3–5] A precondition for this hydrodynamic property is the presence of colloidal particles that pin the contact line preventing it from receding during evaporation.[3,4,9] Fluid flows in a radial direction to replenish solution preferentially lost at the edge where solvent molecules evaporate at the greatest rate. This naturally-occurring phenomenon is easily observed under a microscope with which the two-dimensional radial motion of micron-sized particles can be resolved. The physical basis and flow characteristics of this mass transport system have been previously described.[7,10–12]

Recently, several groups have reported using the primary radial flow to discern information about the components of the solution. Wong *et al.* demonstrated that the size exclusion geometry of the contact line in an evaporating drop can be used for chromatographic separation of colloidal

[a] *Department of Biomedical Engineering, Vanderbilt University, VU Station B 351631, Nashville, TN 37235, USA. E-mail: rick.haselton@vanderbilt.edu; Fax: +1 615 343 7919; Tel: +1 615 322 6622*
[b] *Department of Biochemistry, Vanderbilt University, VU Station B 351631, Nashville, TN 37235, USA*

† Electronic supplementary information (ESI) available: Additional materials provided include a video showing particle motion during drop evaporation from both cross-sectional and top-down viewpoints and a video showing the development of signal in the assay as a function of evaporation time. Four supporting figures are also provided. See DOI: 10.1039/c3lc50991e

particles.[13] Several groups have shown that dried patterns of drops of biological fluids can be used to characterize sample components and potentially be used as an indicator of disease.[14–16] We recently reported a diagnostic assay in which the primary radial flow in an evaporating water drop organizes functionalized magnetic particles to generate a colorimetric response based on the presence of a biomarker.[17] This proof-of-concept assay successfully detected a peptide mimic of the malaria biomarker protein, *Plasmodium falciparum* histidine rich protein (*pf*HRP-II), using a Ni(II)NTA biorecognition element conjugated to the surface of the particles. Evaluation of this assay design reveals several limitations. First, the assay requires precise alignment of the drop over a magnetic field, operationally tedious for what is intended to be a simple and rapid assay. Second, the limit of detection, approximately 200 nM, must be at least 1000× more sensitive for clinical relevance in malaria detection. Finally, the assay does not work in the presence of salt at physiologic levels. Salt crystal formation at the end of the evaporation process significantly alters particle deposition patterns resulting in false results.

Here we describe an assay design based on the secondary flows rather than the primary radial flow to generate an easily detectable signal in an evaporating drop in the presence of the M13K07 bacteriophage, a model target. By relying on these secondary flows rather than the primary radial flow, the design reported here circumvents the limitations of our previously reported assay. Importantly, this revised assay design contains glycerol, which prevents complete drop evaporation and therefore avoids the detrimental effects of salt crystallization. Moreover, this revised assay design relies on an antibody biorecognition element that can be adapted to detect a variety of protein biomarkers rather than the previously used Ni(II)NTA system that has utility specifically for malaria detection.

The secondary flows in an evaporating drop, often referred to as Marangoni flows, are thought to be caused by a surface temperature gradient and corresponding surface tension gradient known as a Marangoni stress.[6–8,18,19] As shown in Fig. 1, fluid flows from regions of low surface tension to high surface tension, which, when superimposed with the temperature gradient, creates symmetrical flow fields through the cross section of the drop (*i.e.* orthogonal to the substrate). These flows can coexist with the primary radial flow and may be either in the same or opposing direction as the primary radial flow.[20] The existence of Marangoni flow in evaporating drops has been previously described.[6–8,18,19] The surface tension of water interfaces is known to be highly sensitive to trace amounts of contaminants, and therefore Marangoni flow in water drops is thought to be limited or non-existent.[8,19]

Unlike primary radial flow which is predominantly two-dimensional and easily imaged with a microscope, Marangoni flow is three-dimensional and requires high frame rate, cross-sectional imaging. Confocal microscopy has been used to track tracer particles in three-dimensional space in an evaporating drop. However, due to a shallow depth of field, confocal microscopy is not currently capable of imaging an entire cross-sectional slice of a colloidal water drop having a height of 300 μm within a time frame that enables particle tracking during drop evaporation.[21,22] Recently, we and others have used optical coherence tomography (OCT) to track particles in an entire cross section of an evaporating drop.[10,23] We recently reported that OCT imaging revealed weak Marangoni flow in evaporating water drops containing 1 μm-diameter polystyrene particles.[10] Under similar experimental conditions, we show here that the addition of glycerol, salt, and surfactant (Tween 20) dramatically enhance this Marangoni flow in water drops evaporated on a PDMS substrate. In this report we use OCT to image this Marangoni flow, which generates signal in the assay by transporting biomarker-induced particle aggregates to the centre of the drop.

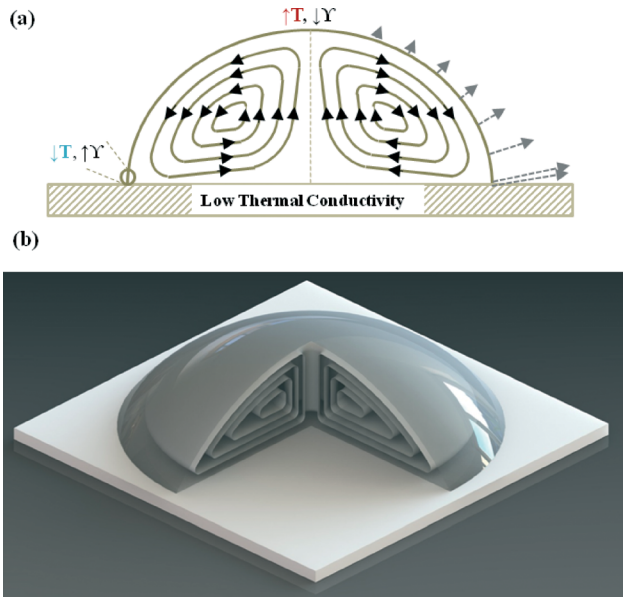

Fig. 1 (a) A non-uniform evaporation rate along the drop surface combined with a low thermally conductive substrate causes temperature (*T*) and surface tension (*Y*) gradients that drive Marangoni flow, which is seen in the video included in ESI,† (b) 3-D rendered drawing of the cross-sectional Marangoni flow in (a) shows radial symmetry around the drop center.

The biosensor design reported here is an immunoagglutination assay in which biomarker-induced particle aggregates are concentrated at the centre of an evaporating drop by Marangoni flow (Fig. 2) rather than concentrated at the edge of the drop by the primary radial flow. The limit of detection is improved by approximately 10^6 times compared to our previously reported assay design that relied on primary radial flow. Also, the assay presented in this study, unlike this previous design, is functional in the presence of physiologic salinity and does not require alignment of the drop over a magnetic field.

Experimental methods and materials

Particle functionalization & characterization

Streptavidin-coated, monodisperse, superparamagnetic particles with a mean diameter of 1 μm were obtained from Life

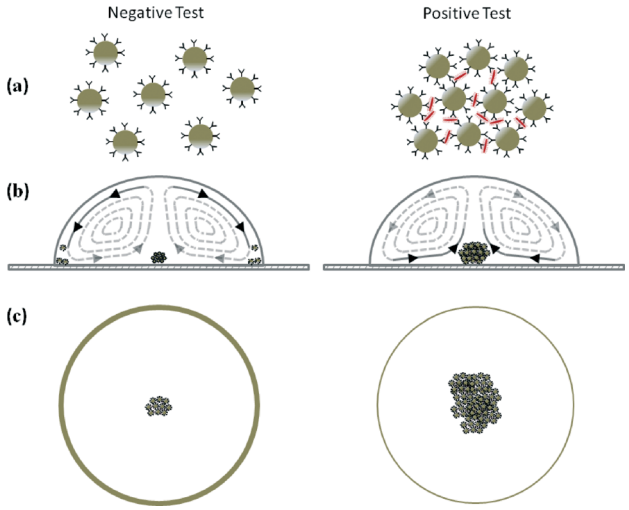

Fig. 2 Schematic of the assay: (a) a sample is mixed with a solution containing 1 μm-diameter particles that are surface-functionalized with αM13 antibody. Particles remain dispersed in the absence of M13 bacteriophage (left), and aggregate in the presence of M13 bacteriophage (right); (b) a 1 μL drop of the reacted solution is deposited on a PDMS substrate. Un-aggregated particles are transported to the drop edge by the Maranogni flow fields while large aggregates settle to the bottom and become concentrated in the centre of the drop; (c) the final deposition pattern of a negative test shows little-to-no aggregates in the centre (left) while a positive test shows an accumulation of aggregates in the centre (right).

Technologies (P/N 656.01). Particles were washed three times with phosphate-buffered saline (PBS, pH 7.4) containing 0.01% Tween 20 and resuspended in the same buffer at a 10× dilution from the stock concentration. Mouse αM13 monoclonal antibody (1 mg mL^{-1} in PBS) was purchased from GE Healthcare (P/N 2792001) and biotinylated with biotinamidohexanoic acid *N*-hydroxysuccinimide ester purchased from Sigma Aldrich (P/N B2673). Unreacted ester groups were subsequently quenched with Tris buffer after a two-hour incubation period. Biotinylated antibody was added to the washed particle solution at an equivalent ratio of 1 mg antibody per 1 mL of stock particles. The particle solutions were then washed with PBS containing 0.01% Tween 20 three times following a two-hour incubation period. Free biotin was then added to the particle solution to bind any unreacted streptavidin on the surface of the particles. After 30 minutes, the particles were then washed three times and stored in PBS containing 0.005% Tween 20 and 0.005% bovine serum albumin (BSA). Control particles were prepared using the same base particle and by reacting with a molar excess of free biotin and then washing three times and storing in PBS with 0.005% Tween 20 and 0.005% BSA. The presence of conjugated antibody on the particles was confirmed by reacting the particles with a α-mouse secondary antibody–horseradish peroxidase conjugate (Sigma Aldrich, P/N A4416), washing three times, and then developing with 2,2′-azino-bis(3-ethylbenzothiazoline-6-sulphonic acid) (ABTS) with hydrogen peroxide. This procedure was repeated for the control particles. Developed solutions turned green for the antibody-conjugated particles and remained clear for the control particles.

Immuno-agglutination assay procedure

Titration assays were carried out in small volume 72-well plates (Nunc, P/N 438733). Plates were first blocked with PBS containing 0.1% Tween 20 and 0.1% BSA, and then rinsed three times with PBS containing 0.1% Tween 20. M13 bacteriophage suspended in PBS was added to the plate and then serially diluted down the rows of the plate with PBS. An equal volume of particle solution containing 3×10^6 particles per μL (in PBS with 0.005% BSA and 0.005% Tween 20) was then added to each well and mixed. An equal volume of water containing 25% glycerol and 0.02% Tween 20 was then added to each well. The final concentration of particles and glycerol in the reaction volume was 1×10^6 μL^{-1} and 8%, respectively. Particle solutions were allowed to react with M13 target for 30 min before depositing drops on the substrate for evaporation and image analysis.

Cross-sectional imaging procedure

A drop (1 μL) of reacted particle solution was deposited on a substrate, and cross-sectional images were recorded with optical coherence tomography (OCT). The procedure and experimental set-up were identical to a previously reported study using a commercial OCT system (Bioptigen, Inc.).[10] The experimental set-up resulted in an optical resolution of approximately 8 μm in the lateral direction, defined as the full-width half-max of the point-spread function of the system, and 6.4 μm in the axial direction. Transverse digital sampling resolution was 3 μm per pixel with an axial digital sampling resolution of 1.69 μm per pixel. OCT files were converted to tagged image file (TIFF) format in Matlab, and ImageJ software was used to edit video sequences and image stacks.

Drop imaging procedure and signal analysis

Evaporated drops were imaged utilizing an Eclipse TE2000-U inverted microscope system (Nikon) with a 10× objective. The slide was front-illuminated using a 144 LED ring light (AmScope). Images of the dried drops were captured using a Zyla sCMOS camera (Andor Technologies) and Elements AR software (Nikon Instruments). During capture, each drop was manually centred in the field of view of the objective and manually focused using focus guides integrated into the software. Final images were captured in 11-bit greyscale at a capture resolution of 0.34 μm per pixel. All images were then processed in Elements to quantify signal in the assay, defined as the area of the aggregates delivered to a pre-defined, concentric region of interest with a diameter of 0.6 times the mean drop diameter.

In order to account for variation in drop size, each drop was measured in Elements by creating a threshold mask of the drop and then measuring the size of the map in pixels. This data was then converted to an equivalent diameter which was used for normalization purposes during processing. After equivalent diameters were calculated, all images were cropped to 340 μm × 340 μm and a circular region of interest with diameter of 340 μm was selected. This region

was selected because it was large enough to encompass central aggregates for all drops, but small enough so as to exclude refraction artefacts occurring at the periphery. Particle identification was then performed on the cropped images with a brightness threshold set at the midpoint of the 11-bit brightness spectrum (luminosity ≥ 1024). In order to exclude free particles and only count aggregates, particle identification was further restricted to include only objects greater than 50 μm in size, a threshold determined in preliminary experiments. This process was performed identically on both αM13-functionalized particles and biotin control samples.

Data was processed by averaging all captured data for each sample at each concentration resulting in n = 15 for each anti-M13 concentration (5 samples in triplicate) and n = 3 (one sample in triplicate) for each biotin control sample. Total particle intensity and mean total particle area were taken from the output of the particle identification process for each drop. These values were normalized to drop size by dividing by drop diameter squared for total particle area and dividing by drop diameter cubed for total particle intensity. Overall means for each test concentration were then calculated as a ratio to mean values for the 0 pM test group and then limit of detection was determined using a logarithmic curve fit and interpolation to calculate the concentration at which projected area and intensity, respectively, would be three standard deviations above the 0 pM mean.

Results and discussion

The assay design investigated here uses Marangoni flow to concentrate target-induced particle aggregates in the centre of an evaporating drop. Unlike the primary radial flow that concentrates colloidal particles at the edge of the drop, the Marangoni flow in the assay reported here travels in the opposite direction and concentrates aggregated particles at the centre of a drop forming an easily detectable spot. Design parameters including substrate material and solution components have been optimized to promote this centre-directed Marangoni flow. Fig. 1a shows a cross-sectional representation of the theoretical Marangoni flow thought to be due to the temperature and surface tension gradients in a drop of evaporating solution.[7] Fluid flows along the substrate toward the centre of the drop then turns toward the air–water interface and flows in the direction of the contact line along the drop surface. This flow pattern is evident in the video in ESI† that shows cross-sectional particle motion in a sequence of OCT images. The surface tension gradient from which these flow fields arise is thought to be caused by a temperature gradient that arises from cooling affects caused by the non-uniform evaporative flux along the drop surface.[3–5] Originally described by Deegan, the evaporation rate of a drop is greatest at the contact line due to the proximal location of ambient, unsaturated gas resulting in non-uniform evaporation along the air–liquid interface.[3–5] The extent to which non-uniform evaporative cooling effects result in a temperature gradient along the drop surface is determined in part by the rate of heat transfer from the isothermal substrate to the air–liquid interface.[20] These heat transfer rates are, in part, a function of both the drop height as well as the thermal conductivities of the substrate and liquid. If the thermal conductivity of the substrate is sufficiently low, then evaporative cooling dominates and causes the lowest temperature to occur at the contact line. Conversely, a highly thermally conductive substrate promotes sufficient heat transfer at the contact line to overcome evaporative cooling effects resulting in the greatest temperature at the drop edge and lowest at the centre. These temperature gradients cause surface tension gradients which in turn drive the Marangoni flow. According to Ristenpart *et al.*, the drop is coolest at the contact line if the substrate has a thermal conductivity less than 1.45 times that of the liquid causing fluid to flow in the direction indicated in Fig. 1a.[20] If the substrate has a thermal conductivity greater than 2 times that of the liquid, the flow direction is reversed. The PDMS substrate used in the research reported here has a thermal conductivity of 0.15 W mK^{-1}, well below 1.45 times the liquid thermal conductivity.[24] According to Ristenpart *et al.*, the resulting flow direction should be the one shown in Fig. 1a. Moreover, these Marangoni flow fields are axisymmetric around the drop centre resulting in a toroidal geometry when viewed from above the drop. Fig. 1b shows a three-dimensional rendering of these flow fields showing this symmetry around the drop centre.

These internal flows and biomarker-induced aggregation are the two basic elements of this approach (Fig. 2). Particles (1 μm diameter) surface functionalized with monoclonal antibodies that bind epitopes on the target biomarker either remain free in solution (Fig. 2a, left) or aggregate in the presence of the bacteriophage target (Fig. 2a, right). Particles become cross-linked in the presence of biomarker resulting in aggregate formation (Fig. 2a, right). In this study, we used the M13K07 bacteriophage as a model biomarker because it is a well characterized vector and its spaghetti-shaped viral capsid is a good cross-linking agent likely to induce aggregation in the assay. When a drop of this particle solution is deposited on a PDMS substrate, Marangoni flow fields circulate particles in solution, shown in the cross section in Fig. 2b. In the absence of biomarker, particles follow these flow fields and are eventually deposited across the substrate surface, predominately at the drop edge resulting in a ring pattern (Fig. 2c, left). In the presence of biomarker, aggregated particles rapidly settle to the substrate and are then transported to the drop centre by the Marangoni flow fields resulting in a concentrated spot (Fig. 2c, right). Due to non-specific particle binding events, a baseline amount of aggregated particles settle at the drop centre in the absence of target biomarker and represents noise in the system.

We have previously described a technique for visualizing cross-sectional flow fields in evaporating drops to characterize and optimize the motion of aggregates in the assay.[10] Optical coherence tomography (OCT) is a real-time, interferometry-based imaging modality in which objects are detected by measuring sample backscatter from a rastered source laser.

With micrometer-scale axial and transverse resolution, millisecond temporal resolution, and a depth-of-field >1 mm, OCT is well-suited to the geometric and time constraints of flow fields in evaporating sessile drops.[10,23,25] Fig. 3 shows time-lapse composite images of an OCT scan through the diameter of a drop containing 0 pM of target (a) and 100 pM target (b). Each image spans 40 s and is generated by overlaying 200 sequential frames captured at a rate of five frames per second. Particles appear as white objects, and flow fields are visualized by the particle tracks that are generated in the composite image. Particles that have reacted with target biomarker in Fig. 3a are aggregated and therefore appear larger than the particles in Fig. 3b that do not have biomarker present. In both Fig. 3a and b, the flow fields are in the direction noted in Fig. 1a and Fig. 2b, *i.e.* toward the contact line along the drop surface and toward the drop centre along the substrate. This direction of motion is more apparent in the time sequence videos included in ESI.† These videos and the composite images in Fig. 3 also show that the flow fields slow down throughout the evaporative process. As water evaporates, the glycerol contained in these drops steadily increases in concentration, which increases solution viscosity and slows the evaporation rate which consequently reduces the surface tension gradient driving the Marangoni flow. This time-dependent change in glycerol also causes a changing refractive index with time. As a result, the OCT images in Fig. 3 contain a shadowing effect at the early time points which is reduced as evaporation progresses. Glycerol is included in the drop solution in order to address the problem of salt crystallization that occurs upon complete evaporation of drops containing a physiologic concentration of salt (0.9%). In preliminary experiments, it was determined that salt crystallization disrupts particle deposition patterns in the absence of glycerol. By including glycerol in the solution, drop evaporation ceases once the water vapour has completely evaporated leaving behind a residual amount of glycerol that prevents salt crystallization.

Importantly, Fig. 3a shows minimal aggregate accumulation at the centre because the particles remain mostly monodisperse in the absence of biomarker. In this case, particles continue to circulate in the Marangoni flow. As we have shown previously, some fraction of these particles becomes entrapped at the air–liquid interface due to surface tension effects and is eventually deposited at the contact line as a result of the outwardly directed flow field along the surface of the drop.[10] Other particles eventually settle along the substrate. Fig. 3b, however shows that large aggregates settle to the PDMS substrate and are transported to the drop centre by the Marangoni flow where the particle aggregates become

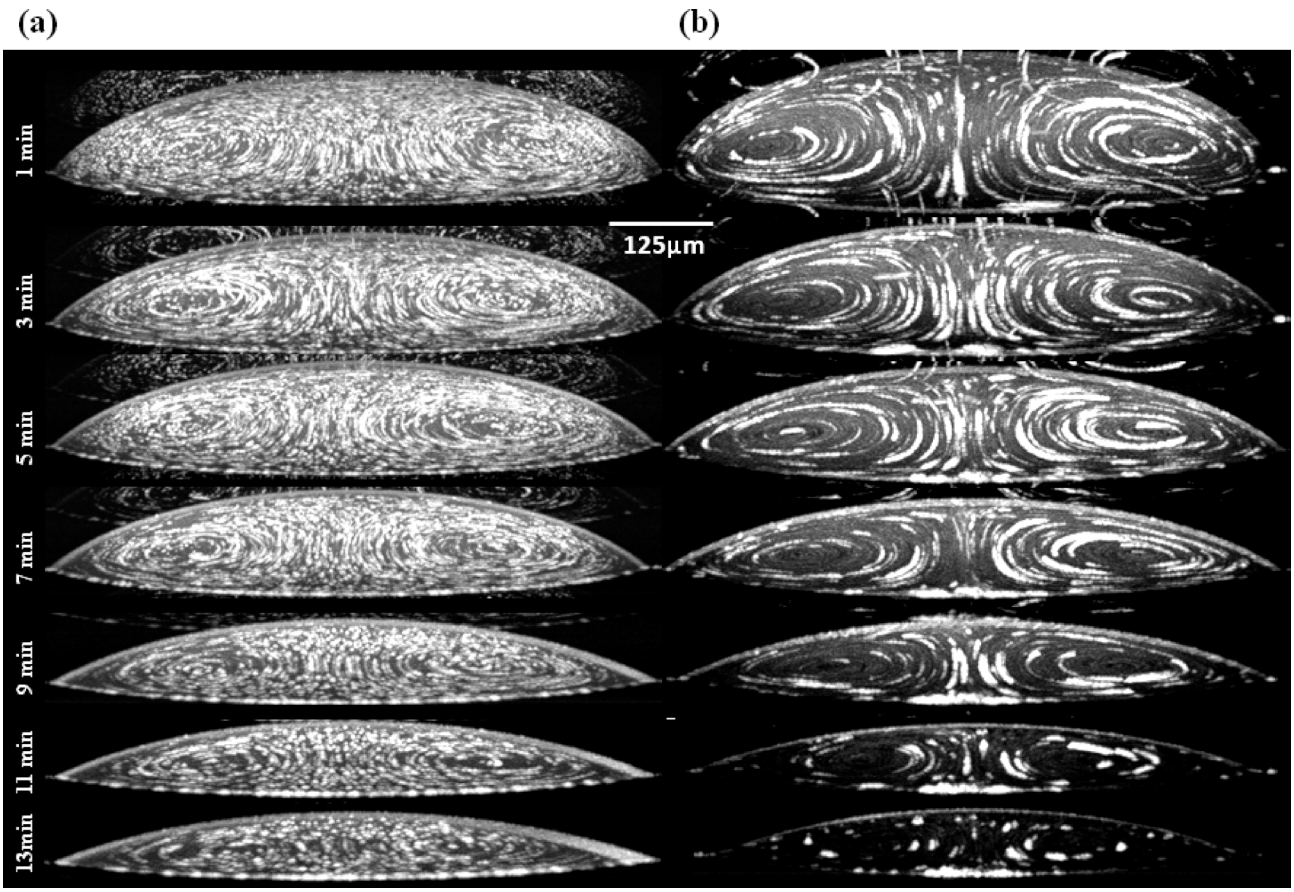

Fig. 3 Time-lapse OCT composites taken through the diameter of an evaporating drop at seven different times during drop evaporation. The time sequence shows the accumulation of aggregates at the bottom centre of a drop containing 10^6 αM13-functionalized particles reacted with 0 pM M13 target (a) or 100 pM of M13 target (b). Each of the composite images consists of 200 consecutive OCT frames acquired at 5 fps.

increasingly concentrated with time. This phenomenon is even more apparent in the video sequences included in ESI.† Consequently, an evaporated drop of particle solution containing biomarker contains greater accumulation of particles at the centre than if no biomarker is present. The final deposition pattern of a 'positive' contains a large spot in the centre, which represents signal in the assay, and appears distinctively different from a 'negative'.

Fig. 4 shows phase contrast micrographs of these final deposition patterns at biomarker concentrations from 0 to 750 pM. The patterns shown in the right panel are a negative control at each corresponding biomarker concentration using particles with a non-reactive surface. These particles are the same as the functionalized particles used in the left panel except surface-coated with biotin rather than αM13 antibody and therefore do not aggregate in the presence of biomarker. The images in Fig. 4 show a general trend of increasing centre spot size with increasing biomarker concentration with the smallest centre spot occurring at 0 pM of biomarker. The deposition patterns at 0 pM biomarker appear essentially the same for the functionalized (left) and control (right). A small spot still appears at the 0 pM concentration due to baseline aggregation that results from non-specific binding between particles. To quantify this aggregation, particle size distributions in the absence and presence of varying amounts of biomarker were optically measured with phase contrast microscopy (ESI†). This background noise could potentially be reduced in future designs by optimizing antibody conjugation techniques so as to maintain a monodisperse particle solution. Additionally, particle size and density parameters could be optimized to reduce this background noise.

Particles that do not aggregate are expected to accumulate at the drop edge. As a result, the ring structure should be larger in the 0 pM sample and biotin controls compared to the −αM13 samples containing M13 target. However, it is not possible to verify this expected result based on the images in Fig. 4 due to refractive and lensing artefact that obscures the ring structure. This artefact is caused by the residual glycerol and the underlying PDMS substrate. Since the particles are not fluorescent, but rather imaged under phase contrast light, it is difficult to characterize the final particle deposition patterns at the drop edge.

Signal in the assay was quantified by optically measuring the total area of aggregates in the centre of the drop as defined by a region of interest (ROI) that was 0.6× the mean diameter of the drops (578 μm). This ROI size was chosen so as to exclude the artefact that occurs near the drop edge due to surface curvature of the fluid and refractive index of the residual glycerol. Signal measurements were subsequently normalized by the drop diameter to adjust for volume variations. Sample drops at each biomarker concentration were deposited in triplicate and signal measurements for the triplicates were averaged. A sample size of five was used in the study for a total number of fifteen drops at each biomarker concentration. Signal-to-noise was then calculated by normalizing assay signal by the baseline signal that is generated in

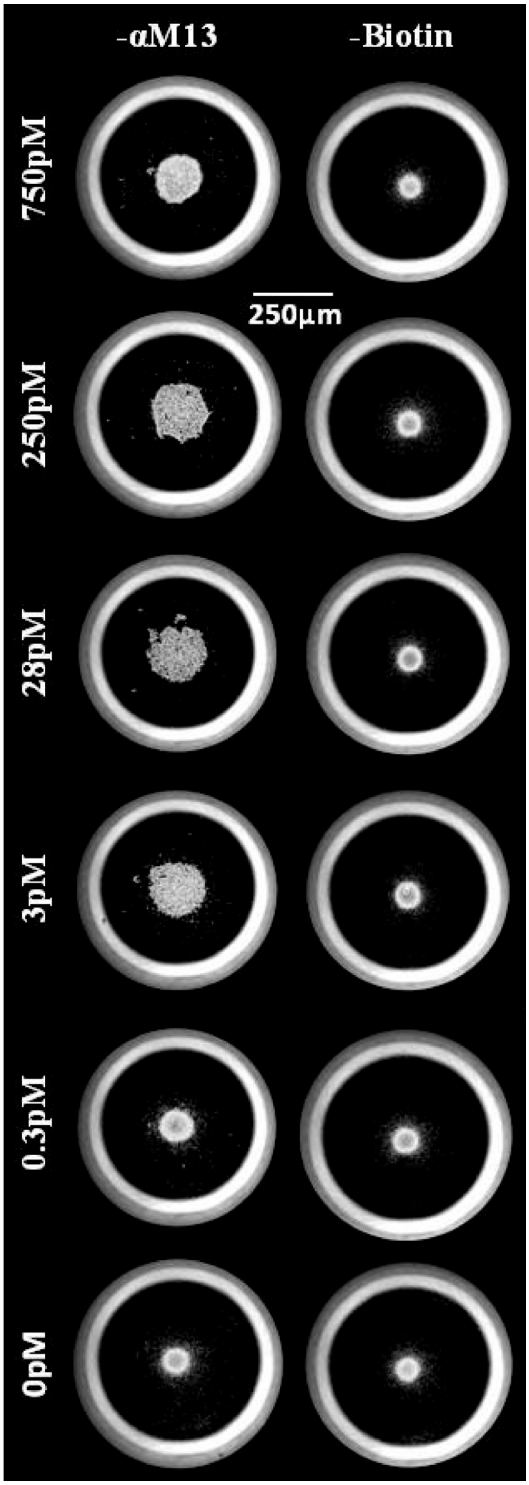

Fig. 4 Change in particle deposition patterns produced by a decrease in M13 target concentration in 1 μL drops containing 10^6 αM13 antibody-functionalized particles (left panel) evaporated on a PDMS substrate. The right panel is a negative control using biotin-coated particles in place of particles functionalized with αM13 antibody. Signal in the assay is seen as a large spot in the centre of the drop at high concentrations of M13 bacteriophage which decreases in size with less M13 bacteriophage (top to bottom). The biotin control particles produce a signal similar in size to the 0 pM sample at all M13 bacteriophage concentrations.

the absence of biomarker. These data are plotted against biomarker concentration in Fig. 5a for both functionalized and control particles. The results show a concentration-dependent signal-to-noise for the functionalized particles that reaches a maximum value of 4.2 at approximately 28 pM of biomarker. Signal-to-noise from the control particles remains statistically indistinguishable from the 0 pM data point which indicates that particle aggregation in the assay is antibody-mediated. The signal-to-noise ratio of the antibody-functionalized particles decreases at greater concentrations of biomarker but remains more than three standard deviations above the control at 750 pM of biomarker.

Signal in the assay increases when aggregated particles are transported by Marangoni flow fields into the centre of the drop. With a fixed number of particles in solution, a greater biomarker concentration results in a greater mean aggregate size and a smaller fraction of un-aggregated particles. However, this relationship reverses when available binding sites on the particles become saturated with biomarker. In this regime of biomarker concentration, aggregation is inhibited by the addition of biomarker because particles no longer compete for available binding sites making particle–particle cross-linking a less probable event. This previously described phenomenon, known as the Hook effect, is the reason why the signal-to-noise in Fig. 5a has a parabolic shape with respect to biomarker concentration.[26,27] As a result, the dynamic range of the assay is limited to approximately four orders of magnitude under the experimental conditions used in this study. This limitation of the assay could potentially be improved in future designs by incorporating a range of antibody-to-particle ratios in the same particle solution. Preliminary data shows that this ratio significantly influences the size distribution of aggregated particles in a titration with biomarker (ESI†). Additionally, the dynamic range of the proposed assay could be improved by evaporating an array of drops whereby the particle solution used in each drop has either a different antibody : particle ratio, or a fixed antibody : particle ratio with a different number of total particles.

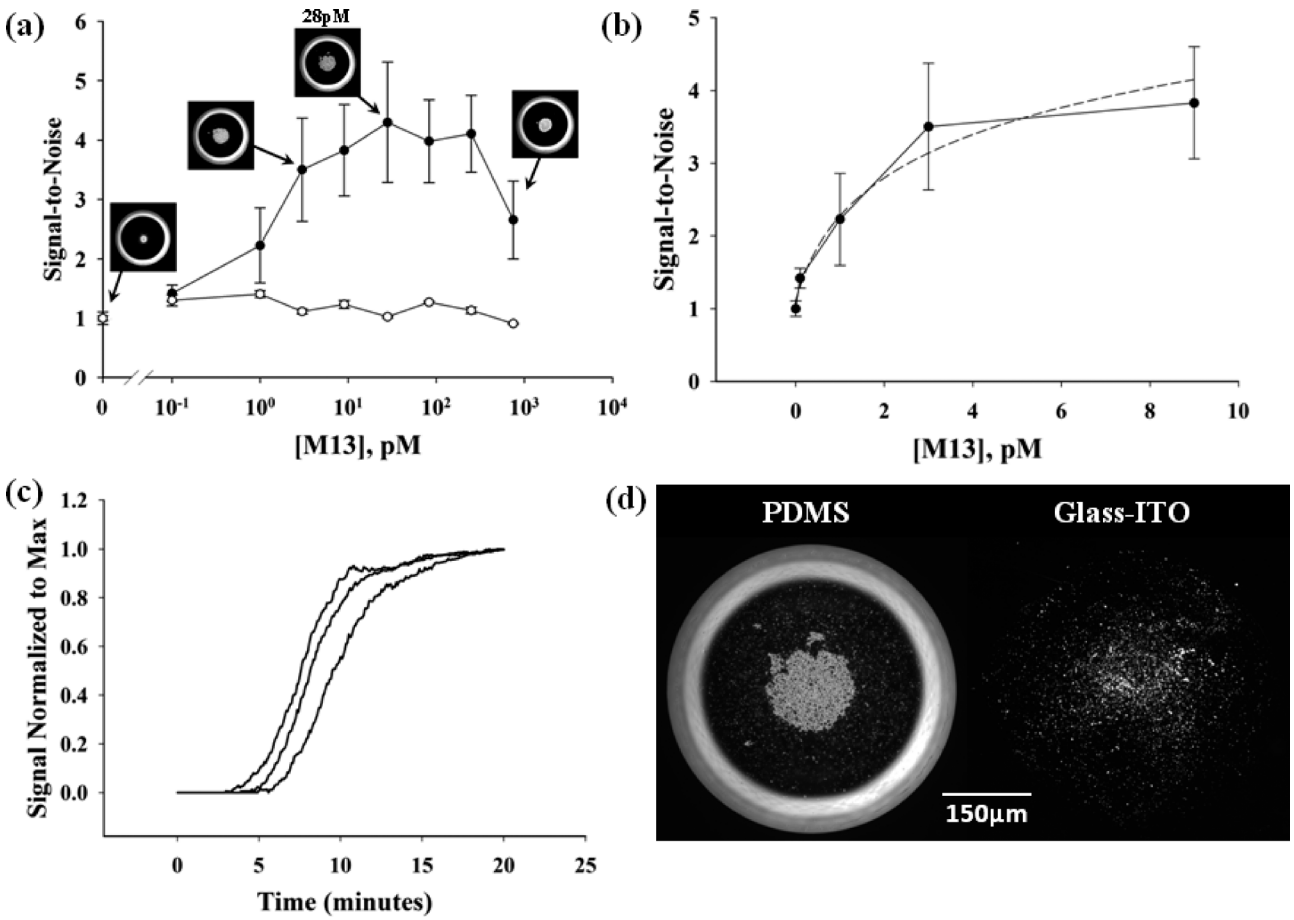

Fig. 5 (a) Signal was measured as a function of M13 target concentration by measuring the area of aggregates in the centre of the drop using a predefined region of interest having a diameter = 0.6 times the mean drop diameter. Signal was normalized for drop volume and divided by the mean 0 pM value to generate a signal-to-noise ratio. Mean values for all M13 target concentrations are plotted (log–linear) for $n = 15 \pm 1\sigma$. (b) Signal-to-noise at the low M13 target concentrations are plotted (linear) for $n = 15 \pm 1\sigma$ and fit with a logarithmic regression (—). (c) Signal-to-noise, normalized to the maximum value for each of three drops containing 28 pM of M13 target evaporated on a PDMS substrate, is plotted as a function of drop evaporation time. (d) Images of particle residue patterns produced by evaporating a drop of αM13-functionalized particles containing 28 pM of M13 target on a PDMS substrate (left) *versus* a glass substrate coated with indium tin oxide (ITO, right).

The lower end of the signal-to-noise data from Fig. 5a is re-plotted in a linear–linear format in Fig. 5b. The limit of detection of the assay was determined by applying a second order curve fit to these data and calculating the lowest biomarker concentration at which signal-to-noise remains at least three standard deviations above the signal at 0 pM of biomarker. This approach indicates a limit of detection of 96 fM. Other methods of signal measurement, including total pixel intensity, number of objects, and mean object diameter, were also evaluated and found not to be as responsive to M13 target concentration as total aggregate area (data not shown).

Signal generation in the assay increases with time. As shown in Fig. 5c, Marangoni flow fields begin transporting settled aggregates to the centre of the drop upon deposition on the PDMS substrate. These Marangoni flows persist until the evaporation-induced surface tension gradient along the surface of the drop is reduced as a result of increasing concentration of residual glycerol. As a result, signal-to-noise in the assay increases throughout drop evaporation and is quantitatively shown in Fig. 5c for three different drops. Signal-to-noise plotted against time shows an initial rise followed by a plateau. The rise is caused by the contribution of two different sources of signal: (1) transportation of aggregates to the centre that have already settled on the substrate, and (2) aggregates circulating in the Marangoni flow that settle to the substrate at the drop centre. The subsequent plateau in these data is due to the diminished flow fields that occur later in the evaporation process. A time sequence of phase contrast images provided in ESI† shows particle aggregates migrating to the centre and the corresponding signal-to-noise as a function of time. The signal-to-noise reaches approximately 80% of maximum within 10 minutes of evaporation. It should be noted that 1 μL drop volumes were used in this study. Since the hydrodynamics scale with drop volume, the time constant of the assay could potentially be lowered by decreasing the drop volume. The trade-off would be detectability of the signal in the assay. At the 1 μL volume, the spot of aggregates that forms in the centre of the assay is visually detectable. However, phase contrast microscopy was used in this study for more precise signal measurement. A likely field implementation of the design would rely on a smart phone to capture an image of the evaporated drop and use a locally-stored image processing app to interpret, quantify, transmit, and store the test result.

The substrate on which the sample drop is evaporated is an important design parameter. Ristenpart *et al.* have conjectured that the presence and direction of Marangoni flow is dependent on the ratio of thermal conductivities of the substrate and drop fluid.[20] A drop of fluid placed on a substrate with sufficiently low thermal conductivity results in a temperature and surface tension gradient that promotes fluid flow along the drop surface directed toward the drop edge. Conversely, a high thermally conductive substrate causes flow in the reverse direction. Therefore, a substrate with sufficiently low thermal conductivity, like PDMS, is required to promote the Marangoni flow in the direction that concentrates biomarker-induced, aggregated particles at the drop centre for detection. According to this theory, a substrate with sufficiently high thermal conductivity produces these flow fields in the opposite direction and therefore will not generate signal in the assay. For example, Fig. 5d shows the deposition patterns produced when a drop containing 28 pM of biomarker is evaporated on a PDMS substrate *versus* an indium tin oxide (ITO)-coated glass slide. The ITO-coated slide has a thermal conductivity of approximately 3.95 W mK^{-1}, significantly greater than the PDMS value of 0.15 W mK^{-1} and sufficiently thermally conductive to generate the reverse flow condition according to Ristenpart *et al.*[20,28] Indeed, the final deposition pattern shown in Fig. 5d is more evenly spread-out along the substrate than that which results on PDMS. However, time composite OCT images of the flow fields that occur in a drop evaporating on an ITO-coated glass slide still show Marangoni flow in the same direction as that produced on a PDMS substrate (ESI†). The Marangoni flow fields on the ITO slide occur at a much slower rate than PDMS, which explains the greater concentration of aggregated particles at the drop centre on PDMS *versus* ITO. However, the reasons for this departure from the Marangoni flow conditions predicted by Ristenpart *et al.* are not entirely clear. Preliminary data show that a drop of particle solution in water evaporated on an ITO-coated slide does not produce Marangoni flow, but a drop of the same particle solution containing glycerol does produce Marangoni flow. In fact, the same observation was made for a PDMS substrate (ESI†) and on a regular glass slide to a lesser degree. The addition of glycerol to an aqueous solution may produce density and viscosity gradients in the evaporating drop that promote Marangoni flow in ways not incorporated in models reported to date.

As previously described, Marangoni flow in an evaporating drop refers to flow fields that result from a surface tension gradient at the air–liquid interface.[3,4,6–8] Deegan first postulated that the non-uniform evaporative flux across the surface of a drop necessarily leads to a corresponding temperature and surface tension gradient.[3,4] This surface tension gradient, which is radially symmetric, causes fluid to flow from regions of low surface tension to high surface tension. Fluid transport across these temperature and surface gradients results in a cross-sectional flow current having toroidal geometry when viewing the drop from above. While this Marangoni flow is prevalent in organic solvents, previous studies have shown that it occurs minimally in aqueous drops presumably because the surface tension of an air–water interface is easily affected by the presence of trace exogenous materials.[8] There have been conflicting reports about the effect of surfactants on Marangoni flow in evaporating drops. One study has shown the presence of surfactants to reduce the surface tension gradient and prevent Marangoni flow.[18] Another group has shown a different type of surfactant molecule to promote Marangoni flow.[19] Drops in this study contain small amounts of the surfactant Tween 20, which may also contribute to the observed flow patterns.

Hu *et al.* have shown using a numerical simulation that the presence of Marangoni flow is dependent on the drop contact angle, which changes with evaporation time.[7] They estimate that the surface tension-induced flow fields cease at contact angles below ~14°. This is thought to be due to the thermal conduction path to the isothermal substrate, which is the primary heat source, becomes sufficiently small at the drop centre, and evaporative cooling at the edge is sufficiently large to eliminate the temperature and surface tension gradients at the drop surface.

Physical and chemical properties of an evaporating drop, like contact angle, non-uniform evaporation rates, and material concentrations, are dynamic and interdependent. Chemical, density, viscosity, temperature, density, and surface tension gradients change with evaporation time and likely affect Marangoni flow fields in ways that are not well understood. These phenomena are the focus of on-going studies.

The design parameters used in this initial biosensor design were chosen to demonstrate proof-of-concept for a low resource point-of-care assay. Several system variables could be optimized for specific future applications. Since the design uses an antibody as the biorecognition element, the assay could be adapted to many different disease types. Here we use the M13K07 bacteriophage as a model target. The bacteriophage, commonly used for phage display, is a spaghetti-shaped viral capsid approximately 700 nm in length with 2800 surface-bound epitopes. The M13 bacteriophage is a good cross-linking agent likely to induce aggregation in the assay because it has a length similar to the diameter of the functionalized particles used in the assay as well an abundance of binding sites. The calculated limit of detection of the assay may be different for different types of biorecognition elements and targets. Additionally, the biosensor could generate a colorimetric signal by incorporating dyed or fluorescent particles. Assay limit of detection and dynamic range may be tuned by optimizing particle size, concentration, and density for a given disease application. The assay design could be further improved by comparing the test result to a control spot and/or evaporating the drop on a functionalized surface that would capture the aggregated particles and enable a rinse step to remove background materials that may obfuscate test interpretation (*e.g.* red blood cells). Finally, the effects of glycerol and surfactant concentrations have not yet been fully elucidated and may be further modified to improve overall biosensor performance. The biosensor investigated in this study has the advantage of using a polydimethylsiloxane (PDMS) substrate, which is commonly used in microfluidics.[29] Therefore this design could potentially be integrated with existing PDMS-based microfluidic architectures, for example droplet-based microfluidic devices. These devices use electrowetting techniques to manipulate the motion and processing of drops on a PDMS surface.[30,31] The approach presented here could potentially be integrated with such technology to provide an optically detectable, multiplexed, and quantifiable test readout strategy.

Conclusions

This work demonstrates the utility of a biosensor design that relies on the hydrodynamics of an evaporating drop to generate an optically detectable test result. This study shows that antibody-functionalized particles aggregate in the presence of biomarker and when a drop of this solution is evaporated on a PDMS substrate, Marangoni flows concentrate the aggregates at the centre of the drop. The substrate material and solution conditions are important design parameters that affect the dynamics of the evaporation-induced flow fields and the extent to which aggregated particles become concentrated in the drop. Signal in the assay is based on the spatial distribution of particle depositions upon drop evaporation. Using standard microscopy to measure the test result, a femtomolar limit of detection is achievable. Future designs may incorporate a camera phone for signal measurement and interpretation, which would be more amenable to a point-of-care diagnostic useful in a low resource setting.

Acknowledgements

This work was supported in part by the Bill and Melinda Gates Foundation through the Grand challenges in Global Health Initiative in Diagnostics as well as a Vanderbilt University Discovery Grant. We gratefully acknowledge Melissa Skala, Ph.D. and David Wright, Ph.D. for valuable discussions.

Notes and references

1 P. Yager, G. J. Domingo and J. Gerdes, *Annu. Rev. Biomed. Eng.*, 2008, **10**, 107–144.
2 P. Yager, T. Edwards, E. Fu, K. Helton, K. Nelson, M. R. Tam and B. H. Weigl, *Nature*, 2006, **442**, 412–418.
3 R. D. Deegan, *Phys. Rev. E: Stat. Phys., Plasmas, Fluids, Relat. Interdiscip. Top.*, 2000, **61**, 475–485.
4 R. D. Deegan, O. Bakajin, T. F. Dupont, G. Huber, S. R. Nagel and T. A. Witten, *Phys. Rev. E: Stat. Phys., Plasmas, Fluids, Relat. Interdiscip. Top.*, 2000, **62**, 756–765.
5 R. D. Deegan, O. Bakajin, T. F. Dupont, G. Huber, S. R. Nagel and T. A. Witten, *Nature*, 1997, **389**, 827–829.
6 L. Y. Barash, T. P. Bigioni, V. M. Vinokur and L. N. Shchur, *Phys. Rev. E: Stat., Nonlinear, Soft Matter Phys.*, 2009, **79**, 046301.
7 H. Hu and R. G. Larson, *Langmuir*, 2005, **21**, 3972–3980.
8 H. Hu and R. G. Larson, *J. Phys. Chem. B*, 2006, **110**, 7090–7094.
9 A. S. Sangani, C. H. Lu, K. H. Su and J. A. Schwarz, *Phys. Rev. E: Stat., Nonlinear, Soft Matter Phys.*, 2009, **80**, 011603.
10 J. R. Trantum, Z. E. Eagleton, C. A. Patil, J. M. Tucker-Schwartz, M. L. Baglia, M. C. Skala and F. R. Haselton, *Langmuir*, 2013, **29**, 6221–6231.
11 H. Hu and R. G. Larson, *Langmuir*, 2005, **21**, 3963–3971.
12 M. T. Harris and E. Widjaja, *AIChE J.*, 2008, **54**, 2250–2260.
13 T. S. Wong, T. H. Chen, X. Y. Shen and C. M. Ho, *Anal. Chem.*, 2011, **83**, 1871–1873.

14 Y. Y. Tarasevich and D. M. Pravoslavnova, *Eur. Phys. J. E: Soft Matter Biol. Phys.*, 2007, **22**, 311–314.
15 Y. Y. Tarasevich and D. M. Pravoslavnova, *Tech. Phys.*, 2007, **52**, 159–163.
16 D. Brutin, B. Sobac, B. Loquet and J. Sampol, *J. Fluid Mech.*, 2011, **667**, 85–95.
17 J. R. Trantum, D. W. Wright and F. R. Haselton, *Langmuir*, 2012, **28**, 2187–2193.
18 R. Savino, D. Paterna and N. Favaloro, *J. Thermophys. Heat Transfer*, 2002, **16**, 562–574.
19 T. Still, P. J. Yunker and A. G. Yodh, *Langmuir*, 2012, **28**, 4984–4988.
20 W. D. Ristenpart, P. G. Kim, C. Domingues, J. Wan and H. A. Stone, *Phys. Rev. Lett.*, 2007, **99**, 234502.
21 H. Bodiguel and J. Leng, *Chem. Eng. Process.*, 2013, **68**, 60–63.
22 H. Bodiguel and J. Leng, *Soft Matter*, 2010, **6**, 5451–5460.
23 S. Manukyan, H. M. Sauer, I. V. Roisman, K. A. Baldwin, D. J. Fairhurst, H. D. Liang, J. Venzmer and C. Tropea, *J. Colloid Interface Sci.*, 2013, **395**, 287–293.
24 K. Eiermann, *Kunststoffe*, 1961, **51**, 512–517.
25 W. Drexler, *J. Biomed. Opt.*, 2004, **9**, 47–74.
26 S. A. Fernando, J. R. Sportsman and G. S. Wilson, *J. Immunol. Methods*, 1992, **151**, 27–46.
27 S. A. Fernando and G. S. Wilson, *J. Immunol. Methods*, 1992, **151**, 47–66.
28 T. Ashida, A. Miyamura, N. Oka, Y. Sato, T. Yagi, N. Taketoshi, T. Baba and Y. Shigesato, *J. Appl. Phys.*, 2009, **105**, 073709.
29 A. Folch, A. Ayon, O. Hurtado, M. A. Schmidt and M. Toner, *J. Biomech. Eng.*, 1999, **121**, 28–34.
30 S. Y. Teh, R. Lin, L. H. Hung and A. P. Lee, *Lab Chip*, 2008, **8**, 198–220.
31 S. K. Cho, H. J. Moon and C. J. Kim, *J. Microelectromech. Syst.*, 2003, **12**, 70–80.

